JOURNAL OF APPLIED CRYSTALLOGRAPHY

Volume 52 (2019)

**Supporting information for article:**

# Development of spin-contrast-variation neutron reflectometry for the structural analysis of multilayer films

**Takayuki Kumada, Kazuhiro Akutsu, Kazuki Ohishi, Toshiaki Morikawa, Yukihiko Kawamura, Masae Sahara, Jun-ichi Suzuki and Naoya Torikai**

**S1. Analytical derivation of $P_H$ from $Q_c$ and oscillation**

The neutrons reflected from the free surface and the interface of a monolayer film with refraction index $n_f$ interfere at the following conditions,

$$2n_f d \sin \theta_f = N\lambda, \quad \text{(S1)}$$

$$2n_f d \sin \theta_f = (N - 1/2)\lambda, \quad \text{(S2)}$$

with

$$n_f^2 = 1-\lambda^2\rho_f/\pi, \quad \text{(S3)}$$

where $d$ is the film thickness and $N$ is the natural number. According to the Snell's law, the refraction angle $\theta_f$ of the neutrons in the film is related to the incident angle $\theta$,

$$n_f \cos \theta_f = \cos \theta. \quad \text{(S4)}$$

$Q$ at the minima of the oscillation, $Q_{min}$, is derived from Equations (S1), (S3), and (S4) for $\rho_f > \rho_{Si}$ or $\rho_f < 0$ as follows,

$$Q_{min} = \frac{2\pi}{d}\sqrt{N^2 + \frac{4d^2\rho_f}{\pi}}, \quad \text{(S5)}$$

but that for $0 < \rho_f < \rho_{Si}$ is given by the Equations (S2)–(S4),

$$Q_{min} = \frac{2\pi}{d}\sqrt{\left(N - \frac{1}{2}\right)^2 + \frac{4d^2\rho_f}{\pi}}. \quad \text{(S6)}$$

$Q_c$ is obtained by substituting $\theta_f = 0$ into Equations (2), (S3), and (S4),

$$Q_c = 4\sqrt{\pi\rho_f}, \quad \text{(S7)}$$

for $\rho_f \geq \rho_{Si}$, and

$$Q_c = 4\sqrt{\pi\rho_{Si}}, \quad \text{(S8)}$$

for $\rho_f < \rho_{Si}$. Figure S3(a) shows $Q_{min}$ and $Q_c$ of the NR curves of the PS film in Figure 2, which are calculated by substituting $\rho_f = \rho_{PS}$ and $d$ = 77 nm into Equations (S5)–(S8). Consistently with the MOTOFIT simulation, $|P_H|$ = 15 ± 6% is determined from the intersection in $Q_{min}$ and $Q_c$ between the SCV-NR curves and the calculated values. The

interval of $Q_{min}$, which corresponds to the oscillation period, decreases with increasing $P_H$ according to the decrease in $\theta_f$ because of Snell's law.

Figure S3(b) shows $Q_{min}$ and $Q_c$ of the NR curves of the strongly annealed PSPI film in Figure 3(a), which are calculated by substituting $d$ = 156 nm and $\rho_f = \rho_{PSPI}$ in

$$Q_{\min} = \frac{2\pi}{d}\sqrt{N^2 + \frac{4d^2(\rho_f - \rho_{Si})}{\pi}}, \quad \text{(S9)}$$

for $\rho_f > \rho_{Si}$ or $\rho_f < 0$,

$$Q_{min} = \frac{2\pi}{d}\sqrt{\left(N - \frac{1}{2}\right)^2 + \frac{4d^2(\rho_f - \rho_{Si})}{\pi}}. \quad \text{(S10)}$$

for $0 < \rho_f < \rho_{Si}$, and

$$Q_c = 4\sqrt{\pi(\rho_f - \rho_{Si})}. \quad \text{(S11)}$$

Here, $\rho_f$ in Equations (S5)–(S7) is replaced by $\rho_f$- $\rho_{Si}$ in Equations (S9)–(S11), respectively, because the neutron beams were irradiated from the rear (Si) side. Consistent with the MOTOFIT simulation, $|P_H|$ = 21 ± 2% is determined from the intersection in $Q_{min}$ and $Q_c$ between the SCV-NR curves and the calculated values.

## S2. MOTOFIT simulation of the hole model

As shown in the microscopy image in Figure S4, the PSPI film has holes whose diameter is ~ 1 μm and their depth is close to one period of the lamellar microdomains of ~20 nm.

Therefore, as shown in Figure S5(a), Mutter *et al.* (1993), and Mutter & Stühn (1995), most of the incident neutrons with the incident angle $\theta = 0.2°–1.5°$ pass through the free surface of the film before being reflected at the bottom of the hole. Therefore, each neutron reflected from the hole interferes with that from the free surface. To simulate the interference using the MOTOFIT program, we used the double flat-surface model in Figure S5(b). In this model, the SLD below the depth of the holes is $\rho_f$, but that above the depth is $(1 - c)\rho_f$, where $c$ is the areal ratio of the holes on the free surface.

**Table S1**: Thickness, SLD, and surface and interface roughness used for the MOTOFIT simulation of the PS film in Figure 2.

| | Thickness (nm) | SLD ($\times 10^{10}$ cm$^{-2}$) | | | Roughness (nm) |
|---|---|---|---|---|---|
| | | UNR | pSCV-NR ($P_H$ = +16%) | nSCV-NR ($P_H$ = -16%) | |
| Vacuum | - | 0 | | | - |
| PS | 77 | 1.48 | 2.67 | 0.29 | 1.2 |
| SiO | 1.36 | 3.47 | | | 1.1 |
| Si | - | 2.07 | | | 0.5 |

**Table S2**: Thickness, SLD, and surface and interface roughness used for the MOTOFIT simulation of the strongly annealed PSPI film in Figure 3(a).

| | Thickness (nm) | SLD ($\times 10^{10}$ cm$^{-2}$) | | | Roughness (nm) |
|---|---|---|---|---|---|
| | | UNR | pSCV-NR ($P_H$ = +21%) | nSCV-NR ($P_H$ = -21%) | |
| Si | - | 2.07 | | | - |
| SiO | 1.36 | 3.47 | | | 0.5 |
| PSPI | 156 | 0.83 | 2.70 | -0.95 | 1.0 |
| Vacuum | - | 0 | | | 4.0 |

**Table S3**: Thickness, SLD, and surface and interface roughness used for the MOTOFIT simulation of the weakly annealed PSPI film in Figure 3(b).

| | Thickness (nm) | SLD ($\times 10^{10}$ cm$^{-2}$) | | | Roughness (nm) |
|---|---|---|---|---|---|
| | | UNR | pSCV-NR ($P_H$ = +8%) | nSCV-NR ($P_H$ = –8%) | |
| Vacuum | - | 0 | | | - |
| PI | 4.46 | 0.28 | 1.07 | -0.51 | 3.93 |
| PS | 9.07 | 1.48 | 2.08 | 0.89 | 3.61 |
| PI | 10.66 | 0.28 | 1.07 | -0.51 | 3.89 |
| PS | 11.96 | 1.48 | 2.08 | 0.89 | 2.12 |
| PI | 11.36 | 0.28 | 1.07 | -0.51 | 2.10 |
| PS | 9.05 | 1.48 | 2.08 | 0.89 | 2.64 |
| PI | 5.79 | 0.28 | 1.07 | -0.51 | 4.97 |
| SiO | 1.36 | 3.47 | | | 1.11 |
| Si | - | 2.07 | | | 0.5 |

**Table S4**: Thickness, SLD, and surface and interface roughness used for the MOTOFIT simulation of the strongly-annealed PSPI film in Figure 4(a).

| | Thickness (nm) | SLD ($\times 10^{10}$ cm$^{-2}$) | | | Roughness (nm) |
|---|---|---|---|---|---|
| | | UNR | pSCV-NR ($P_H$ = +21%) | nSCV-NR ($P_H$ = -21%) | |
| Si | - | 2.07 | | | - |
| SiO | 1.36 | 3.47 | | | 0.5 |
| PSPI | 126 | 0.83 | 2.70 | -0.95 | 1.0 |
| PSPI with 20% hole | 28 | 0.66 | 2.16 | -0.76 | 10 |
| Vacuum | - | 0 | | | 3.5 |

**Table S5**: Thickness, SLD, and surface and interface roughness used for the MOTOFIT simulation of the weakly annealed PSPI film in Figure 4(b).

| | Thickness (nm) | SLD ($\times 10^{10}$ cm$^{-2}$) | | | Roughness (nm) |
|---|---|---|---|---|---|
| | | UNR | pSCV-NR ($P_H$ = +8%) | nSCV-NR ($P_H$ = –8%) | |
| Vacuum | - | 0 | | | - |
| PI with 40% hole | 4.46 | 0.17 | 0.64 | -0.31 | 3.95 |
| PS with 40% hole | 9.07 | 0.89 | 1.25 | 0.53 | 3.02 |
| PI | 10.66 | 0.28 | 1.07 | -0.51 | 3.90 |
| PS | 11.96 | 1.48 | 2.08 | 0.89 | 2.01 |
| PI | 11.36 | 0.28 | 1.07 | -0.51 | 2.49 |
| PS | 9.05 | 1.48 | 2.08 | 0.89 | 4.95 |
| PI | 5.79 | 0.28 | 1.07 | -0.51 | 2.69 |
| SiO | 1.36 | 3.47 | | | 1.10 |
| Si | - | 2.07 | | | 0.5 |

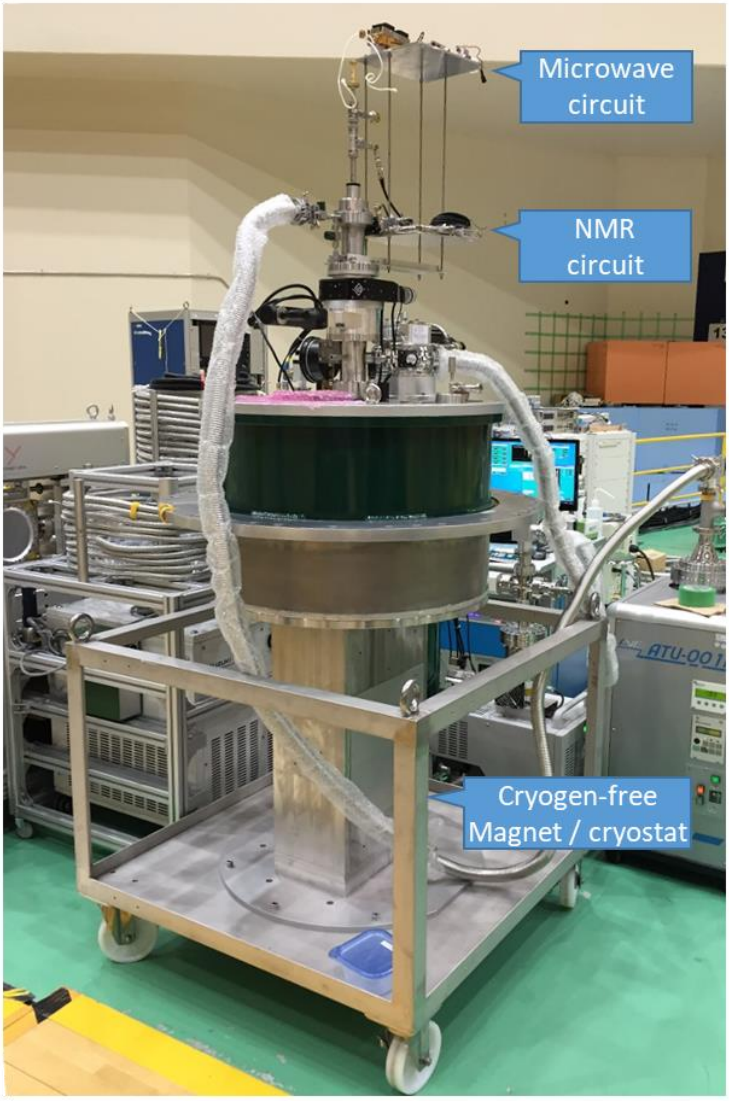


**Figure S1**: DNP apparatus.

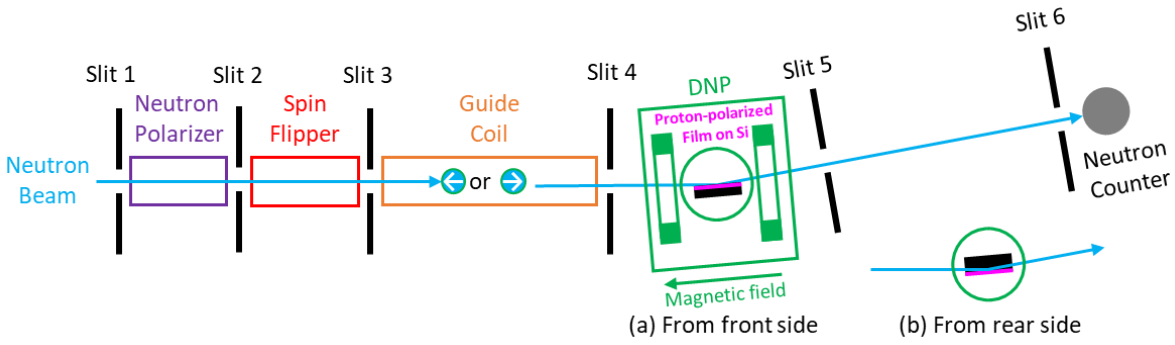


**Figure S2:** Layout of the SCV-NR measurement.

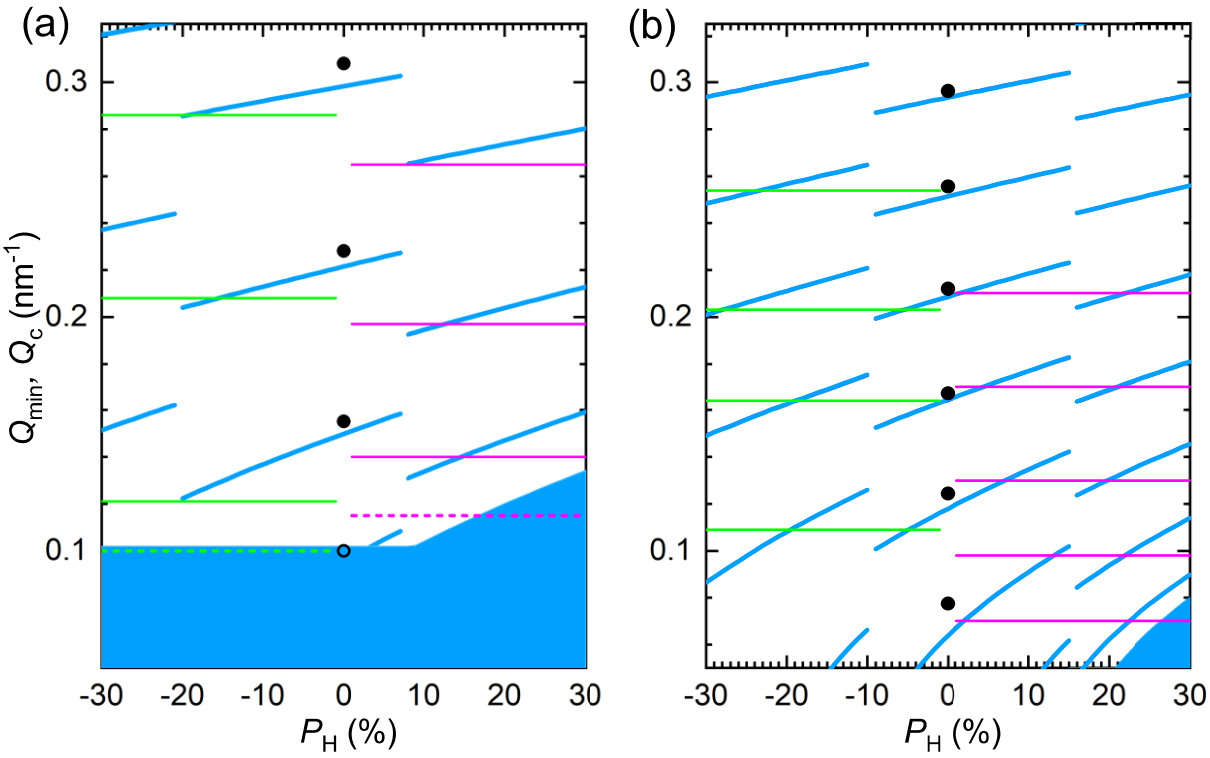


**Figure S3:** $Q_{min}$ (solid) and $Q_c$ (dashed) of (a) the PS film in Figure 2 (green) and (b) the strongly annealed PSPI film in Figure 3(a) (magenta). Blue bold lines, $Q_{min}$ calculated by substituting $d$ = 77 nm in Equations (S5) and (S6) in (a) and 155 nm in Equations (S9) and (S10) in (b); boundary with blue filled area, $Q_c$ from Equations (S7) and (S8) in (a) and Equation (S11) in (b); closed and open circles, $Q_{min}$ and $Q_c$ of the UNR curve, respectively.

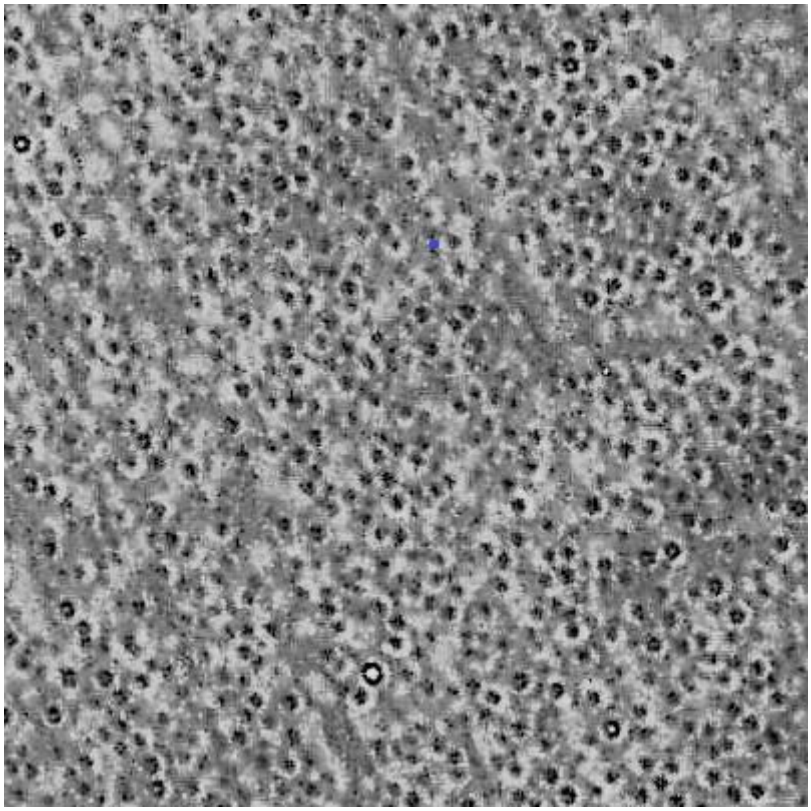

**Figure S4**: Optical microscopy image of the weakly annealed PSPI film using Keyence VHX-500. Length of a side is 80 μm. According to the results of X-ray reflectivity by Mutter et al. (1993) and Mutter and Stühn (1995), the micrometer-sized black dots are attributed to the holes.

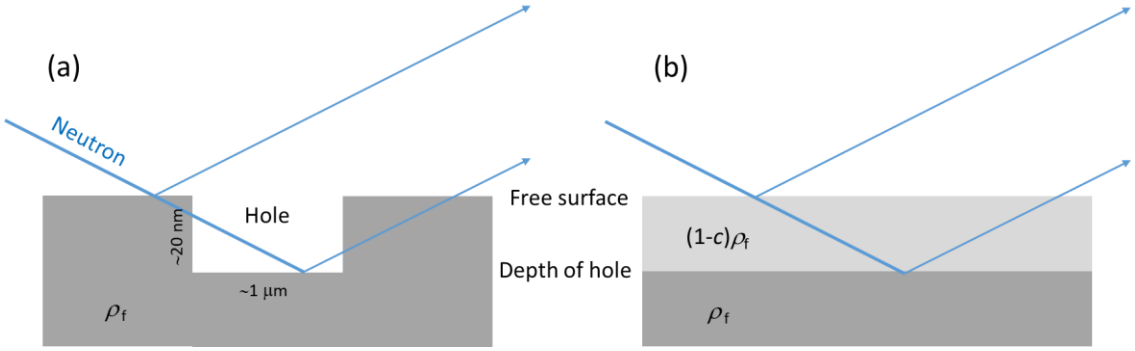


**Figure S5**: Superposition of neutrons reflected at the free surfaces and bottom of the holes. According to Mutter and Stühn (1995), the double flat-surface model (b), which has a flat layer with a depth of the hole and SLD of (1-c)$\rho_f$, is used to simulate reflections from the surface having holes with the a real occupation ratio *c* (a).